NeuroImage 158 (2017) 406–416

Contents lists available at ScienceDirect

NeuroImage

journal homepage: www.elsevier.com/locate/neuroimage

Phase properties of transcranial electrical stimulation artifacts in electrophysiological recordings

Nima Noury [a,b,*], Markus Siegel [a,*]

[a] Centre for Integrative Neuroscience & MEG Center, University of Tübingen, Germany
[b] IMPRS for Cognitive and Systems Neuroscience, Tübingen, Germany

ARTICLE INFO

Keywords:
Transcranial electric stimulation (tES)
Transcranial alternating current stimulation (tACS)
Transcranial direct current stimulation (tDCS)
EEG
MEG
Neural entrainment
Stimulation artifacts

ABSTRACT

Monitoring brain activity during transcranial electric stimulation (tES) is an attractive approach for causally studying healthy and diseased brain activity. Yet, stimulation artifacts complicate electrophysiological recordings during tES. Design and evaluation of artifact removal methods require a through characterization of artifact features, i.e. characterization of the transfer function that defines the relationship between the tES stimulation current and tES artifacts. Here we characterize the phase relationship between stimulation current and tES artifacts in EEG and MEG. We show that stimulation artifacts are not pure in-phase or anti-phase signals, but that non-linear mechanisms induce steady phase deflections relative to the stimulation current. Furthermore, phase deflections of stimulation artifacts are slightly modulated by each heartbeat and respiration. For commonly used stimulation amplitudes, artifact phase deflections correspond to signals several times bigger than normal brain signal. Moreover, the strength of phase deflections varies with stimulation frequency. These phase effects should be accounted for during artifact removal and when comparing recordings with different stimulation frequencies. We summarize our findings in a mathematical model of tES artifacts and discuss how this model can be used in simulations to design and evaluate artifact rejection techniques. To facilitate this research, all raw data of this study is made freely available.

1. Introduction

Current neuroscience in humans largely relies on correlative approaches. Thus, manipulative techniques to precisely interfere with human brain function are much needed. Transcranial Electric Stimulation (tES) is a non-invasive brain stimulation technique, applicable to both healthy and diseased subjects, in which a weak electrical current is applied to the subject's head (Fertonani and Miniussi, 2016; Nitsche and Paulus, 2000). Despite promising behavioral effects of tES, its use in both forms of direct and alternating current stimulation (tDCS and tACS, respectively) has been mainly restricted to behavioral and after effect studies (Kuo and Nitsche, 2012; Soekadar et al., 2016; Thut et al., 2017). This is because strong stimulation artifacts interfere with simultaneous electrophysiological recordings (Noury et al., 2016).

Recently, several approaches to monitor brain activity during tES by means of EEG and MEG have been proposed (Helfrich et al., 2014; Neuling et al., 2015; Soekadar et al., 2013; Voss et al., 2014; Witkowski et al., 2016). Several of these efforts are based on artifact removal techniques that aim to dissociate brain signals from stimulation artifacts. These techniques, as well as computer simulations and phantom experiments employed to design and evaluate these techniques, are based on critical assumptions about stimulation artifacts. If these assumptions are wrong, this may lead to misleading results and wrong interpretations when trying to dissociate human brain signals and tES artifacts from EEG and MEG (Noury et al., 2016). Thus, a thorough understanding of stimulation artifacts is needed to prevent pitfalls of simultaneous tES-M/EEG research and to pave the way for new artifact removal methods. Importantly, this understanding of stimulation artifacts is also needed to verify artifact removal methods by means of phantoms or computer simulations.

Recently, we characterized the amplitude of tES artifacts and showed that, contrary to previous assumptions, for both EEG and MEG, tES artifacts do not simply reflect stimulation currents, but that heartbeat and respiration strongly modulate the strength of stimulation artifacts in a non-linear fashion and cause a time-varying mapping between stimulation current and tES artifacts (Noury et al., 2016). Here, we extend our previous work by characterizing the phase properties of tACS stimulation artifacts.

* Corresponding authors. Centre for Integrative Neuroscience, University of Tübingen, Otfried-Müller-Str. 25, 72076 Tübingen, Germany.
E-mail addresses: nima.noury@cin.uni-tuebingen.de (N. Noury), markus.siegel@uni-tuebingen.de (M. Siegel).

http://dx.doi.org/10.1016/j.neuroimage.2017.07.010
Received 23 February 2017; Received in revised form 14 June 2017; Accepted 9 July 2017
Available online 12 July 2017

2. Materials and Methods

2.1. Participants and experimental protocol

All experiments were conducted in 5 healthy male participants, were carried out in accordance with the Declaration of Helsinki, and were approved by the local ethics committee. All subjects gave written informed consent before participating. 4 subjects participated in 6 experimental runs of the main tACS experiment with small stimulation electrodes. EEG and MEG signals were recorded during the entire experiment. Each run consisted of the following sequential conditions: sham, tACSa, tACSb, sham, tACSb, tACSa. Each condition was 66 s, and tACSa and tACSb were randomly assigned to 11 Hz and 62 Hz tACS. In the first 5 runs, subjects were fixating at a central fixation spot (60 Hz monitor refresh rate) and in the last run they were asked to close their eyes.

To check the influence of stimulation electrode size on the artifact's phase, we performed a control experiment with large rubber electrodes in one subject (6 experimental runs similar to the main experiment, subject 2). In another control experiment in the same subject, we recorded one experimental run with only MEG signals recorded during application of tACS with large rubber electrodes (no EEG cap attached to the subject, eyes open). The aim of this control experiment was to check for potential noise effects of the EEG device on the MEG system. We performed one more control experiment on another single subject (subject 5) to check for the potential influence of the EEG ground electrode placement on the stimulation artifact. The recording and stimulating electrode layout was the same as the layout in the main tACS experiment. In this control experiment, we applied 62 Hz tACS and continuously and recorded 10 min of EEG with ground on the right forearm and 10 min of EEG with ground on the forehead (Fpz of 10-10 system), while the subject fixated a central fixation spot.

2.2. Transcranial electric stimulation

Stimulation current was applied with an IZ2h stimulator (Tucker Davis Technologies Inc.) with 0.5 mA amplitude (i.e., 1 mA peak-to-peak for tACS). None of the subjects reported any flicker percept. For the main experiment, stimulation was applied through two standard Ag/AgCl EEG electrodes over right occipital and right parietal areas (electrodes O10 and CP4 of the 10-10 electrode system). For the control experiment with large electrodes, 35 cm^2 MR-compatible rubber electrodes (neuroConn GmbH) were placed over occipital and frontal lobes underneath the EEG cap. For all experiments, stimulation electrodes were attached using Ten20 conductive paste (Weaver and Company) and their impedance was kept below 2.5 kΩ. To minimize magnetic artifacts produced by the stimulation current, we carefully twisted all stimulation cables.

2.3. Data acquisition and preprocessing

We simultaneously recorded 72-channel EEG (NeurOne system, Mega Electronics Ltd) and 272-channel MEG (Omega, 2000; CTF Systems) throughout all experiments at 10,000 Hz and 2343.8 Hz sampling rate, respectively. EEG electrodes were positioned based on the 10-10 electrode system using an EEG cap (EC80, EASYCAP). All signals were in the dynamic ranges of the recording systems and no clipping was observed for either EEG or MEG signals.

EEG electrodes were attached using Abralyt 2000 conductive gel and impedances were kept below 2.5 kΩ for most electrodes. In the main experiment, we referenced EEG electrodes to FCz, while in the control experiment with large rubber electrodes signals were referenced to Fz, because of the placement of the stimulation rubber electrodes. The ground electrode was positioned on the right forearm, except for one control experiment with 10 min of ground electrode placement on the forehead. We did not apply any offline re-referencing to the EEG recordings. Along with EEG and MEG, we recorded the stimulation (injected) current, vertical EOG (two electrodes above an below the right eye), ECG, and respiratory movements using bipolar channels of the EEG system. The injected current was measured by recording the voltage drop across a 200 Ω resistor positioned in series to the head. The ECG was recorded through 2 electrodes placed below the right clavicle and below the left pectoral muscle. Respiration was continuously recorded with a piezo respiratory belt transducer (Vermed-Medizintechnik).

2.4. Eye blinks

We applied a zero-phase 6th order Butterworth low-pass filter at 4 Hz to the difference of the vertical EOG channels, and visually inspected the result to find the moments of eye blinks. Application of a low-pass filter was necessary, because during 11 Hz tACS strong stimulation artifacts mask the effect of eye blinks. All intervals with eye blinks were removed from the phase signals.

2.5. Artifact phase shift

For each EEG and MEG channel, we defined the temporal artifact phase-shift signal as the phase shift between each channel's signal and the injected current. As the injected current was recorded with the EEG system, for calculating the phase shift of the MEG channels, we used an MEG-synchronized version of the injected current (see below). The original injected current recorded with the EEG system was used for the EEG channels. We first band-pass filtered the signals using a 6th-order zero-phase Butterworth filter centered at the stimulation frequency of interest with a pass-band of ±5 Hz. After band-pass filtering, we down-sampled signals to 1 000 Hz and 781.25 Hz, respectively for EEG and MEG, and applied the Hilbert transform to obtain phase signals. Finally, we subtracted the un-wrapped phase of the injected current form the un-wrapped phase of each channel. For all comparisons between sham and tACS conditions, we used the filter and injected current of the corresponding tACS condition. To test the significance of the phase shift of each channel, we calculated phase shifts of 1 000 white noise signals with the same procedure as applied to the recorded signal for the corresponding condition, and compared the circular standard deviation of each channel's phase shift over time with the population of circular standard deviations of the noise phase signals.

EEG recordings corresponding to the reference channel by definition contain only measurement noise. Therefore, we excluded this channel from all following analyses.

2.6. Phase deflection

For each channel, we calculated the circular mean of the phase shift over time and defined the phase deflection as the smallest value among the phase mean subtracted by 0, π and -π.

To test the significance of the phase deflection of each channel, we applied a permutation test. First, we calculated the phase deflection from 0, π or -π at each time point (the temporal average of this signal is the phase deflection, as defined above). Band-pass filtering around the stimulation frequency induces a dependency of phases at nearby time points. To take into account this dependency, we re-sampled the phase deflection signal at 2 Hz, i.e. substantially below the bandwidth of the pass-band (±5 Hz). We then computed the p-value of the null-hypothesis of zero phase deflection, by comparing the absolute of the temporal average of this signal against the distribution of the absolute of temporal averages of 1 000 random phase deflection signals. These random signals were generated by randomly assigning a sign to the phase deflection at each time point.

We defined the effective strength of phase deflections as the strength of a sine signal that could have generated these phase deflections, when added to a sinusoidal artifact with no phase deflection. To find such a sine signal, for each channel and each stimulation frequency, we calculated the difference between a sine wave with zero-phase and a sine wave with

the observed phase deflection, and multiplied the result with the mean artifact amplitude. Finally, we calculated the standard deviation of this signal and compared it against the standard deviation of sham recordings (the sham signal was band-passed filtered with a 6th order Butterworth filter centered at the stimulation frequency of interest with a pass-band of ±5 Hz). We applied a similar procedure to quantify the effective strength of phase jitters over time. We calculated the difference between a sine wave with zero-phase and a sine wave with mean-removed phase signal (i.e. containing only the phase jitter) of each channel, multiplied the result with the mean artifact amplitude of each channel, and divided the variance of this signal by the variance of the sham recording.

To test the effect of tACS frequency on phase deflections, for each channel, we calculated the ratio between the absolute value of phase deflections of the two stimulation conditions, found the median across all channels and subjects, and compared this value to the distribution of 1 000 randomly generated values. These random values were generated by applying the same procedure with condition labels randomly assigned to the phase deflections.

2.7. MEG-synchronized injected current

Because the stimulation current was recorded with the EEG system, we generated the MEG-synchronized version of the stimulation current by estimating and correcting the differences in system clocks and temporal offsets between the MEG and EEG systems based on trigger codes that were simultaneously sent to both systems. We first generated two time vectors, representing moments that triggers were received by EEG and MEG systems. Next, we performed a linear regression to find the best scale and shift parameters that map MEG time to EEG time. Using these parameters, we estimated the corresponding EEG time points for the moments at which the MEG system sampled the data, and finally resampled the injected current at these time points to find the rate-corrected version of the injected current.

This procedure corrected for the difference between EEG and MEG clock rates, and most of the temporal offset between the two systems. However, the resulted rate-corrected injected current still contained a small temporal offset relative to the MEG signals. This offset was either due to a difference of hardware-induced delays between EEG and MEG signals (e.g. due to anti-aliasing filters), or due to a small difference in how fast MEG and EEG hardware register the received trigger codes. We estimated this temporal offset based on the increase in the phase difference between the rate-corrected injected current and MEG signals from 6.99° to 38.85° (median across channels and subjects), when the stimulation frequency increases from 11 Hz to 62 Hz. These phase values correspond to a temporal offset of 1.7 ms between the MEG signals and the rate-corrected injected current. Therefore, we generated the MEG-synchronized injected current by shifting the rate-corrected injected current by 1.7 ms.

2.8. Temporal analyses

To find the effect of heartbeats on artifact phase signals, we first found the R-peaks of each subject's simultaneous ECG, defined 4 s long segments of the phase shift signal centered on the R-peaks, and averaged all these segments. To assess the significance of each subject's heartbeat related modulation, for each channel we calculated the power of the average heartbeat-locked phase signal at the frequency of the subject's average heart rate by means of the discrete-time Fourier transform. Next, we assigned a p-value to this power value based on the histogram of 1 000 power values generated with the same procedure but using random R-peak moments. The resulting p-values were corrected for false discovery rate (FDR; Benjamini and Hochberg, 1995). We studied the temporal dynamic of the heartbeat-locked phase modulations by means of PCA. PCA was applied only to the average heartbeat-locked phase modulation of those channels that showed significant heartbeat-locked phase modulations. Finally, we estimated the effective strength of these phase modulations. For each channel, we generated two 4 s long sinusoids, one with no phase modulation and the other one with the measured average heartbeat-locked phase modulation, subtracted them from each other, multiplied the result with the channel's average artifact strength (the standard deviation of each channel's signal over time), and compared the standard deviation of this residual signal with the standard deviation of the sham recordings.

We applied the same procedure to check the effect of respiration on 8 s long segments centered on inspiration endpoints.

2.9. Spectral analyses

We estimated the power spectra of sham and tACS conditions on 4 s long segments. We first split the data in 4 s long segments, applied a Hanning window to each segment, computed the Fourier transform of each segment, and calculated the average power across segments. To study the influence of the artifact's phase modulation on the artifact's power spectrum (Fig. 3e, j), we first estimated the average heartbeat-locked phase modulation as explained above. Then we constructed two 4 s long 62 Hz sine waves: one without phase modulation and one with the average heartbeat-locked phase modulation. We scaled both sine waves with the average artifact strength of the relevant channel. Finally, to check the influence of the phase modulation on the power spectrum, we subtracted the non phase-modulated signal from the phase-modulated signal and calculated the power of the Fourier transform of the residual.

2.10. Influence of pure amplitude modulation

Heartbeat and respiration strongly modulate the strength of artifact signals (Noury et al., 2016). To make sure that these amplitude modulations do not influence Hilbert transformation and phase estimations in a way that leads to the observed heartbeat and respiration locked phase effects, we repeated the temporal analysis on a fake phase signal. For each channel and each stimulation condition, we excluded the actual phase of signals and generated waveforms that only reflected the amplitude modulations of the recordings. This was done by calculating each signal's amplitude by means of Hilbert transform and multiplying it with the injected current. Finally, we obtained the fake phase signals by estimating phase of the resulted waveforms.

2.11. Heartbeat simulation

We checked if a combination of EEG referencing, small random phase shifts on each EEG electrode (i.e. the random capacitive effect), and heartbeat-locked artifact amplitude modulations might generate heartbeat-locked artifact phase modulations (Fig. 5c). We first re-referenced EEG recordings to average reference to estimate the tACS artifact of each EEG electrode prior to referencing to Fcz. By means of Hilbert transform, we found the artifact amplitude at each EEG electrode, segmented it into 4 s long pieces centered at each ECG R-peak, and computed the average heartbeat-locked artifact amplitude modulation at each EEG electrode. For each electrode, we then multiplied this amplitude signal onto a 4 s long sine wave at 11 Hz, which had a small constant random phase drawn from a uniform distribution from 0 to 0.05 radians. This specific interval was chosen because the absolute value of phase deflections of the 10 percent of channels with strongest artifact amplitudes were lying in an interval of about 0.05 radians. The rational behind this selection is that, based on the model presented in Fig. 5a, phase deflections of channels with strong artifacts should mostly reflect the capacitive effect of the EEG electrodes. Next, we simulated the effect of referencing by simply subtracting the signal of the desired reference electrode from all other electrodes. Finally, for each channel we estimated the temporal phase modulation by means of Hilbert transformation, and quantified the modulation strength as the temporal standard deviation of the phase modulation in radians. We repeated this

simulation 100 times and calculated the mean across all simulations.

2.12. Heartbeat and respiration frequencies

For each subject, heartbeat and respiration rates were defined as the inverse of the median of the temporal intervals between successive ECG R-peaks and inspiration endpoints, respectively.

2.13. Analysis software

All data analyses were performed in Matlab (MathWorks) using custom scripts, the open source toolbox Fieldtrip (Oostenveld et al., 2011), and the circular statistics toolbox (Berens, 2009).

2.14. Raw data

The raw data analyzed here is the same as the data analyzed in our previous study (Noury et al., 2016), and is available by contacting: noury.siegel.2017@gmail.com.

3. Results

3.1. Anti-phase regions of artifact

We recorded EEG and MEG during 11 Hz tACS, 62 Hz tACS, and sham stimulation in 4 subjects. Stimulation currents were injected through two Ag/AgCl electrodes with 1 mA peak-to-peak strength (Fig. 1a). EEG was recorded through the 72 remaining electrodes of the 10-10 electrode system, along with 272 MEG channels. Throughout the experiment, we also recorded the electrocardiogram (ECG) and respiration of subjects.

The stimulation current leaves one tACS electrode, runs through the entire head, and reaches the other tACS electrode. Therefore, all EEG electrodes experience strong sinusoidal stimulation artifact. The artifact's amplitude topography reflected the location of the stimulation and reference electrodes (top topographies in Fig. 1b and c). This is because, for each EEG channel, the EEG device measures the voltage difference between that EEG electrode and the reference electrode. Due to this subtraction, one expects that the artifact phase divides EEG channels into two anti-phase groups. To test this, we calculated the phase difference between each EEG signal and the stimulation current. All channels showed significant phases relative to the stimulation current and, as

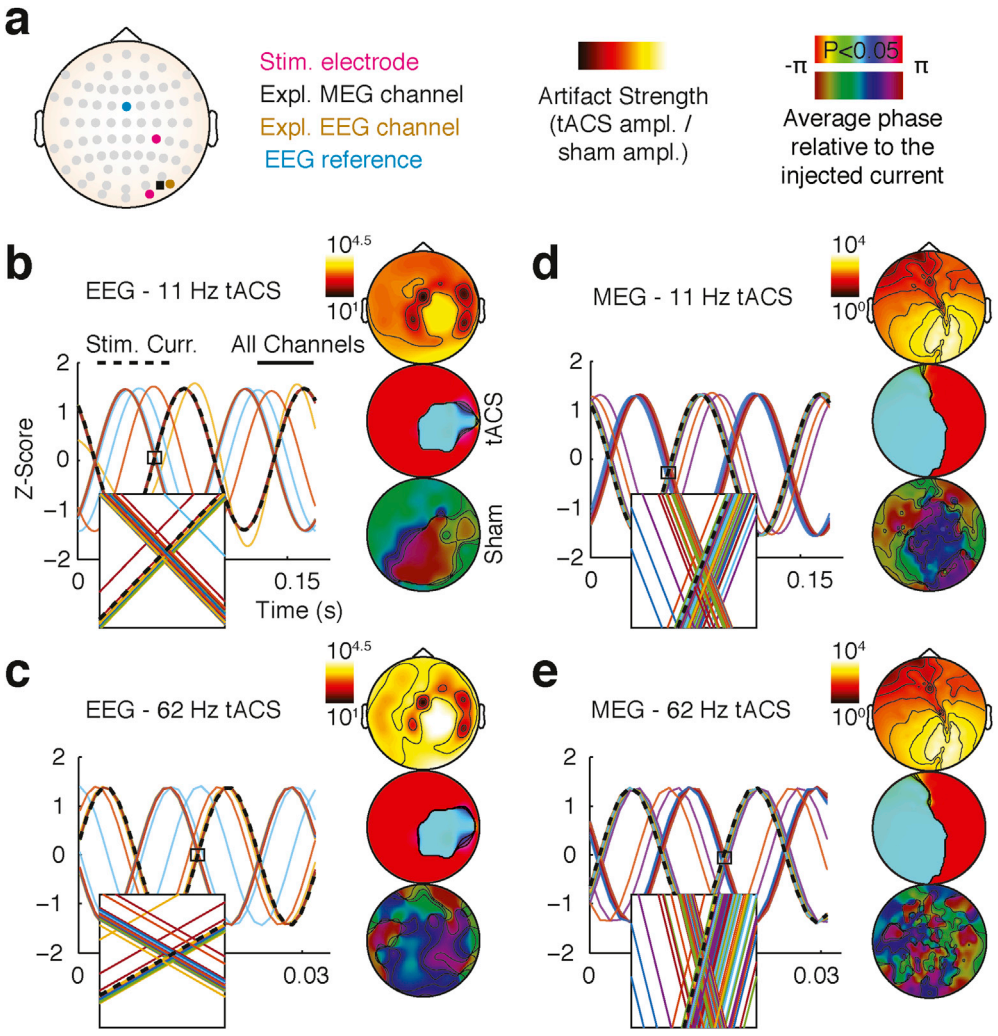

Fig. 1. tACS experiment and artifact phase. (a) 74 Ag/AgCl electrodes were placed according to the 10-10 system. Two electrodes (purple circles) were used for tACS stimulation and the all other electrodes were used for EEG measurement. The brown circle and black square indicate the channels used for demonstrating the EEG (O9) and MEG (MLT31) results in the next figures, respectively. The blue circle shows the reference EEG electrode. (*b*) Typical EEG and (*d*) typical MEG recordings during 11 Hz tACS. Time domain plots show 2 cycles of normalized signals of all channels (solid lines) and stimulation current (dashed lines). Subplots show the zero-crossing moment. Notably, different channels cross the zero line at different moments. The top topography shows the artifact strength relative to sham recordings, i.e. the standard deviation of signals recorded during tACS divided by the standard deviation of sham recordings, in logarithmic scale. Middle and bottom topographies depict the average phase shift of each channels signal relative to the stimulation current. Bright colors indicate regions with significant phase shift. (*c*) and (*d*) show recordings during 62 Hz tACS. The data shown is from the first subject.

expected, the phase topography reflected two anti-phase regions (Fig. 1b and c, blue and red regions in middle topographies).

For the MEG, the main sources of artifacts are the inward and outward currents running through the stimulation cables and the scalp. Due to the opposite current direction of inward and outward currents, artifact phase should be divided into two anti-phase regions. Indeed, similar to EEG, all MEG channels showed significant phase shifts relative to the stimulation current, and the phase topography was divided into two anti-phase regions (middle topographies in Fig. 1d and e). As a simple control, we checked whether band-passed sham recordings show any significant stable phase throughout the experiment. We did not find a significant phase in any EEG or MEG channel during sham condition (bottom topographies in Fig. 1b, c, d, e).

3.2. Artifact phase deflections in EEG and MEG

If EEG and MEG signals at the stimulation frequency were reflecting a purely linearly transformed version of the stimulation current, each channel's signal had to be on average either an in-phase (0° phase shifted) or an anti-phase (180° phase shifted) version of the stimulation current. To test this, we quantified each channel's phase deflection from such a pure in-phase or anti-phase signal (Materials and Methods). For almost all EEG and MEG channels this revealed an average phase deflection that was significantly different from 0° or 180° with small jitters over time (subplots in Figs. 1 and 2a, d, $p < 0.05$ Bonferroni-corrected for multiple comparisons across channels, for properties of phase jitter see Supplementary Fig. 1).

Do these average phase deflections from pure linear artifacts reflect the effect of tACS on brain activity, or are they due to nonlinear technical artifacts? We hypothesized that if the observed phase deflections were due to technical artifacts, their value should be related to the artifact's strength. Indeed, for both, EEG and MEG and for both tACS conditions, we found a significant negative correlation between the strength of the tACS artifact and strength of the phase deflection (Fig. 2b, e; Spearman correlation (r) of −0.32 and −0.26, for EEG, and −0.51 and −0.61, for MEG, $p < 1e^{-6}$, pooled across subjects and channels). To further address this question, for each channel we quantified the effective strength of phase deflections as the smallest sinusoidal signal that, when added to an artifact with no phase deflection (pure in-phase or anti-phase), could lead to the observed phase deflection (Materials and Methods). Next, we compared the strength of these sinusoids to the strength of sham recordings in the same frequency band (Fig. 2c, f). For most of the channels the sinusoids that would have to be added to a purely linear artifact were more than 10 times bigger that the normal EEG and MEG signals (79% and 94% of EEG channels and 18% and 69% of MEG channels for 11 Hz and 62 Hz tACS, respectively). As none of the subjects experienced phosphenes or other sensations during the experiment, we concluded that the brain could not have generated such strong sinusoids. We concluded that the observed phase deflections are part of the stimulation artifacts (see the next section for a third observation supporting this conclusion).

We tested if the phase deflections of the two stimulation conditions were related to each other. In both EEG and MEG, phase deflections of 11 Hz and 62 Hz tACS artifacts were strongly correlated across sensors (Spearman correlation (r) of 0.79 and 0.85 for EEG and MEG, respectively; both $p < 10^{-16}$). Next, we investigated if the strength of phase deflections changes with tACS frequency. For both, EEG and MEG we found a significant change in phase deflections by increasing the stimulation frequency from 11 Hz to 62 Hz. For EEG, the median of ratios of absolute phase deflections (62 Hz divided by 11 Hz) across channels was 0.84, suggesting a general decrease of phase deflections, while the median of ratios across MEG channels was 1.32, suggesting an increase in phase deflections ([10th, 90th] percentile of [0.4, 1.39] and [0.56, 4.48] for EEG and MEG, respectively; all $p < 1e\text{-}3$, permutation test, Materials and Methods).

3.3. Heartbeat-locked phase modulations

Heartbeats move the head and EEG electrodes and influence the electrical properties of the body (Kristiansen et al., 2005; Nyboer et al., 1950; Pinheiro et al., 2010). Consequently, heartbeats modulate the amplitude of tES stimulation artifacts for EEG and MEG (Noury et al., 2016). Therefore, we hypothesized that heartbeats also modulate the phase of the stimulation artifact. To test this, in each subject we checked whether the artifact phase in EEG and MEG shows a rhythmic modulation locked to the subject's ECG R-peak (Materials and Methods). Indeed, in all subjects and for both, 11 Hz and 62 Hz tACS, most channels showed a significant rhythmic modulation of their artifact phase ($P < 0.05$, FDR

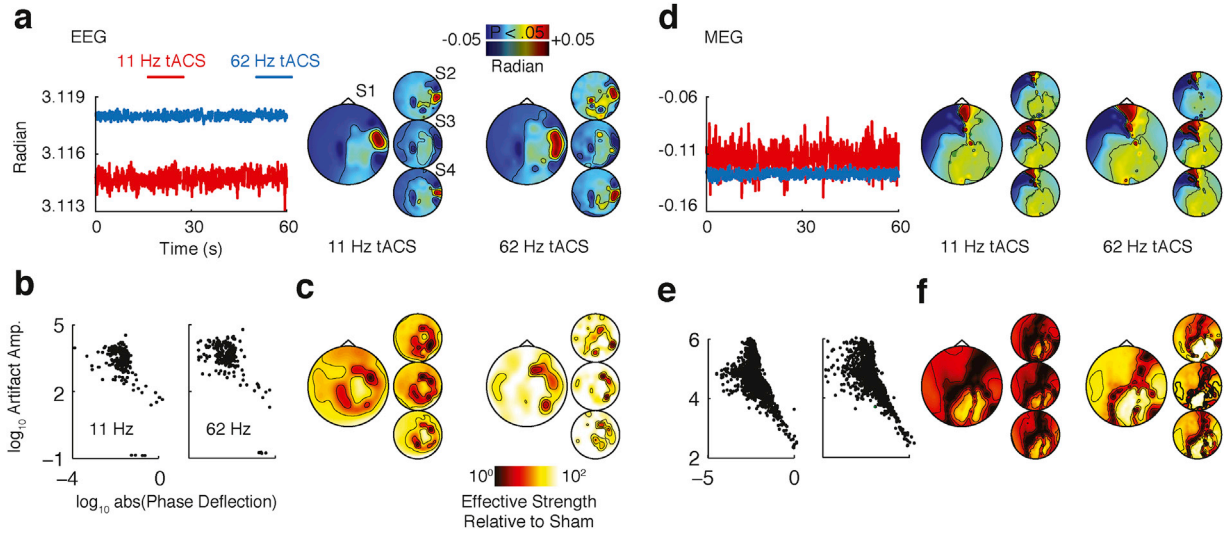

Fig. 2. Artifact phase deflection. (*a*) Artifact phase deflection in EEG. Time domain plot shows 1 min of artifact phase shift relative to the stimulation current during 11 Hz (red) and 62 Hz (blue) tACS (channel O9 of the first subject). Topographies show the phase deflection for each channel in radians. Almost all channels show significant phase deflections (non-significant regions are masked at $P = 0.05$ corrected). (*b*) Relation between artifact strength (standard deviation of signals during tACS) and absolute value of phase deflection in log-log scale. Data from all subjects is shown. Each point corresponds to a single channel in one subject. (*c*) Effective strength of phase deflections relative to sham recordings. Topographies show, in logarithmic scale, how big the signal is that results from the artifact deflection from pure in-phase or anti-phase linear artifacts, relative to the signal during sham recordings. (*d-f*) Artifact phase deflection properties in MEG. Same conventions as in (*a-c*). The time domain plot in (*d*) shows results from channel MTL31 in the first subjects. Bigger topographies correspond to the first subject (S1) and smaller topographies correspond to all other subjects (S2-S4).

corrected, Fig. 3a, b, f, g). Heartbeat-locked phase modulations were clearer for 62 Hz tACS as compared to 11 Hz (topographies in Fig. 3a, b, f, g), which might be due to weaker physiological signals mixing with the artifact at 62 Hz. In the frequency domain, these phase modulations spread the stimulation artifact beyond the stimulation frequency (Fig. 3e, j). This is because frequency is proportional to the temporal derivative of phase. Due to the heartbeat-locked phase modulations, the temporal derivative of the artifact's phase is not constant. Therefore, in the frequency domain, several frequencies are contaminated with the stimulation artifact. In other words, similar to the influence of the artifact's amplitude modulation (Noury et al., 2016), the artifact's phase modulation results in broadband artifacts.

To characterize the temporal dynamic of the spatial pattern of heartbeat-locked modulations, in each subject we applied PCA to the average heartbeat-locked phase modulations (Fig. 3c, h, Materials and Methods). In each subject, at least 2 of the first 3 PCs showed rhythmic dynamics and the first 3 PCs explained more than 99% and 97% of the variance for EEG and MEG, respectively. Consequently, the spatial pattern of phase modulations is not constant over time, but shows rhythmic temporal changes. Moreover, this suggests that for simulating tES artifacts, simulated phase modulations should contain at least 2 PCs.

The strength of heartbeat-locked phase modulations tended to be stronger for channels with bigger artifact phase deflections. For both EEG and MEG, we found a strong positive correlation between the modulation strength and absolute value of the artifact phase deflection (spearman correlation (r) of 0.56 and 0.64, for EEG, and 0.5 and 0.5, for MEG, for 11 Hz and 62 Hz tACS, respectively; all $p < 10^{-9}$). Furthermore, we found that for both, MEG and EEG and for both stimulation frequencies across channels, the strength of the heartbeat-locked phase-modulation was negatively correlated with the overall strength of tACS artifacts (spearman correlation (r) of −0.78 and −0.55, for EEG, and −0.85 and −0.69 for MEG, for 11 Hz and 62 Hz tACS, respectively; all $p < 10^{-16}$). These effects provide additional evidence for the interpretation that the observed phase deflections are caused by nonlinear artifacts, and not by brain activity.

Heartbeat-induced phase modulations were in the range of milliradians (Fig. 3a, b, f, g). Therefore, we asked if the effect of these small phase modulations is negligible, or if they should be considered in design and evaluation of artifact removal techniques. To answer this, we quantified each channel's modulation strength, in analogy to how we quantified the effective strength of average phase deflections before (Fig. 3d, i, Materials and Methods). For many channels, heart-beat locked phase modulations lead to artifact signals bigger than 10% of the EEG and MEG signals, and in some channels, in particular for MEG, the effect of heartbeat-locked phase modulations was as big as the signals recorded without stimulation. In sum, heartbeat-locked modulations of the artifact's phase induced sizable artifacts that should be accounted for in the design and evaluation of artifact removal techniques.

Heartbeats modulate artifact amplitudes in both EEG and MEG (Noury et al., 2016). Therefore, we checked if these amplitude modulations may influence our phase estimations such that the observed phase modulations may merely reflect these amplitude modulations. We simulated the case of stimulation artifacts with only amplitude modulation (Materials and Methods) and repeated the heartbeat-locked phase analysis on the estimated phase of these simulated artifacts. None of the EEG or MEG channels showed any significant heartbeat-locked phase modulation ($p > 0.05$, FDR corrected). Thus, we concluded that the observed phase-modulations did not merely reflect heartbeat locked amplitude modulations.

3.4. Respiration-locked phase modulations

Similar to the heartbeat, also respiration moves the head and EEG electrodes, modulates body impedance, and modulates tES artifact amplitudes (Dornhorst et al., 1952; Michard, 2005; Noury et al., 2016; Pinheiro et al., 2010). Thus, we expected to observe respiration-locked modulations of artifact phase, similar to heartbeat-locked effects. Indeed, for many channels, respiration-locked segments of artifact phase showed significant rhythmic modulations with sensor topographies similar to heartbeat-locked modulations (Supplementary Fig. 2). Compared to heartbeat-locked phase modulations, respiration-locked phase modulations reached significance in fewer channels, which may be due to the lower number of respirations as compared to heartbeats.

3.5. Ground electrode

We investigated whether the position of the EEG ground electrode could have generated the artifact phase-features observed in EEG recordings. To this end, in one subject we recorded two sessions of a 62 Hz tACS control experiment with EEG ground positioned either on the forearm or forehead. The two recordings showed similar artifact phase deflection and heartbeat-locked phase modulations (Supplementary Fig. 3). Thus, we concluded that artifact phase features in EEG are not related to the position of the EEG ground electrode.

3.6. Stimulation electrode size

In one subject, we performed another control experiment with big rubber stimulation electrodes to test if the observed features of the artifact phase might be due to the size of our stimulation electrodes (Fig. 4). For both, EEG and MEG and for both, 11 Hz and 62 Hz tACS, we found artifact phase deflection and phase modulations similar to the experiment with small stimulation electrodes. Thus, we concluded that the observed features are not related to the stimulation electrode size.

3.7. MEG without EEG

As the EEG cap and recording device may potentially generate noise on the MEG recordings, we checked if the artifact phase features observed in MEG were due to the simultaneous EEG measurements. In one subject, we recorded 2 min of MEG per tACS condition, without the EEG cap (Materials and Methods). We observed phase features in the recorded MEG data that were similar to the phase features observed during simultaneous MEG and EEG recordings (Supplementary Fig. 4). Thus, we concluded that the observed MEG phase effects were not related to the simultaneous EEG recordings.

4. Discussion

Here, we provide, to the best of our knowledge, the first characterization of the phase relationship between stimulation current and tACS artifacts in EEG and MEG. We show that tACS artifacts are not simple sinusoids at either 0 or 180° phase relative to the stimulation current, but that each channel shows a frequency dependent phase deflection. The magnitude of this phase deflection is negatively correlated with the amplitude of tACS artifact. Moreover, we show that the artifact phase is modulated by heartbeat and respiration. These phase modulations result in weak tACS artifacts at frequencies beyond the stimulation frequency. To facilitate research on tES artifacts and artifact rejection methods, all raw EEG and MEG data used in this study is made available online.

4.1. Artifact's bandwidth

The artifact's phase modulations spread stimulation artifacts beyond the stimulation frequency (Fig. 3e, j). This is in general similar to the effect of artifact's amplitude modulations, which result in broadband stimulation artifacts contaminating the power spectrum up to ±10 Hz beyond the stimulation frequency for a stimulation current of 1 mA peak-to-peak (Noury et al., 2016). It should be noted that the effective strength of phase modulations (Fig. 3d, i and Supplementary Fig. 2) is on average about hundred times smaller than the effective strength of amplitude modulations (Figs. 3 and 4 of Noury et al., 2016). In other words,

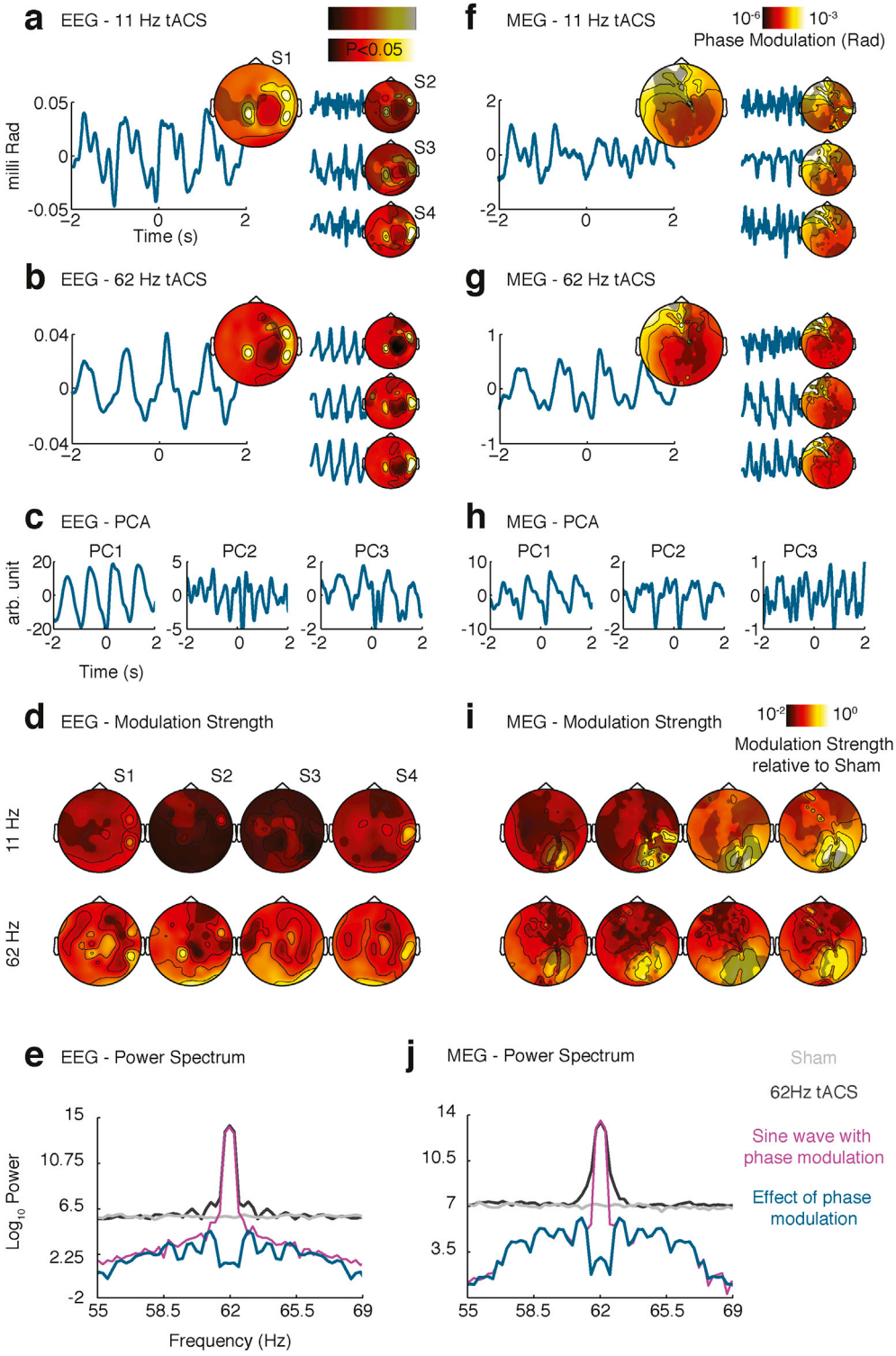

Fig. 3. Heartbeat-locked artifact phase modulation. (*a*) The time courses show how on average the EEG phase-shift relative to the stimulation current modulates around the time of heartbeats during 11 Hz tACS (signal from channel O9). The topography shows the modulation strength quantified as the decadic logarithm of the standard deviation of average heartbeat-locked phase modulation (non-significant modulations are masked at P = 0.05 corrected). The large panel shows data from subject S1. Smaller panels show all other subjects. (*b*) Similar to (*a*), but for 62 Hz tACS. (*c*) First 3 principle components (PCs) of a PCA applied to the average heartbeat-locked phase modulation. Only channels with significant heartbeat-locked modulations are included in the PCA. Data from 62 Hz tACS condition of the first subject. (*d*) Topographies show the effective strength of heartbeat-locked phase modulations, relative to the strength of sham recordings in decadic logarithmic scale. (*e*) Influence of the artifact's phase modulation on the artifact's power spectrum. Light and dark gray curves depict average power spectra of recordings from sham and 62 Hz tACS conditions, respectively (EEG channel O9). The magenta curve shows the power spectrum of a sine wave with constant amplitude and time-varying phase. The phase of this wave was set equal to the heartbeat-locked phase modulations of the same channel. The blue curve shows the effect of phase modulations in the frequency domain, i.e. the power spectrum of the residual signal, when a pure sine wave with no phase modulation is removed from the sine wave with phase modulations. (*f-j*) Same conventions as for (*a-e*), but for MEG recordings. Figures (*f, g, j*) depict results from channel MTL31.

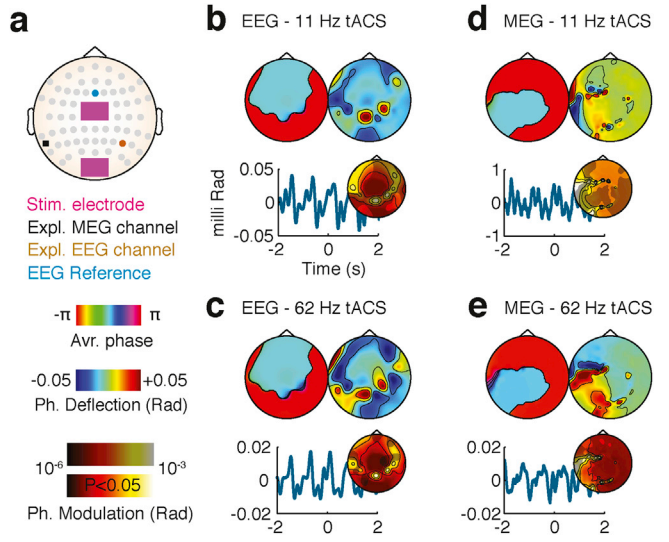

Fig. 4. tACS artifact phase properties for large stimulation electrodes. (*a*) Two large rubber stimulation electrodes (purple squares) were positioned between 62 EEG electrodes placed according to the 10–10 system. The brown circle and black square indicate the position of channels used for demonstrating EEG (P6) and MEG (MLT54) results, respectively. The blue circle shows the reference EEG electrode. (*b*) EEG artifact phase during 11 Hz tACS. The top left topography shows the average phase shift relative to the stimulation current. As expected, this topography is divided into two anti-phase regions. The top right topography shows artifact phase deflections from linear artifacts. Similar to tACS with small stimulation electrodes, different channels' artifacts deflect from linear artifacts. Bottom panel shows the heartbeat-locked phase modulation. The topography shows the standard deviation of phase modulation in decadic logarithmic scale (non-significant modulations are masked at P = 0.05 corrected). (*c*) As (*b*), but for 62 Hz tACS. (*d-e*) As (*b-c*), but for MEG recordings.

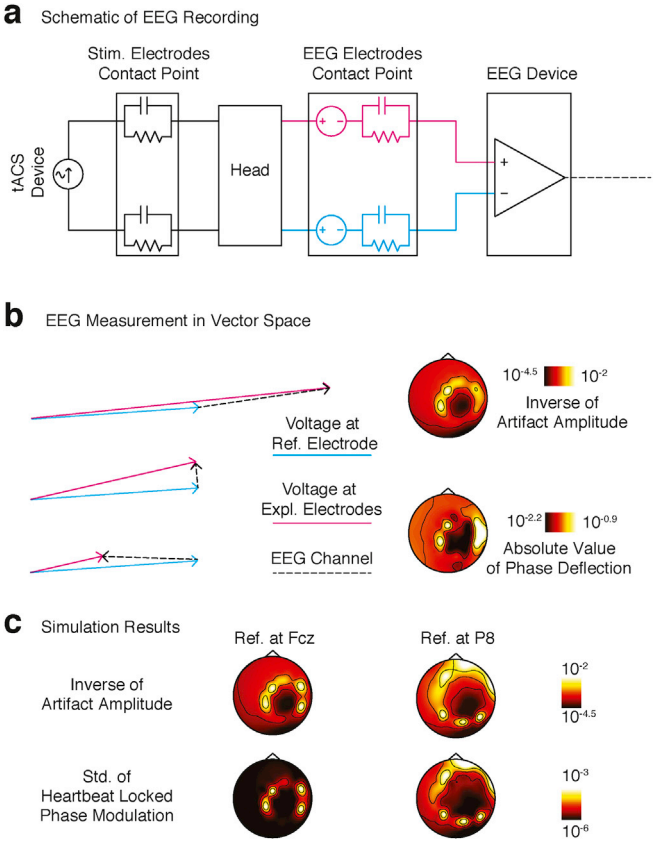

Fig. 5. EEG artifact phase. (*a*) Schematic diagram of tACS stimulation and EEG recordings. The stimulation current leaves the tACS device, flows through the head, and returns to the tACS device. The EEG device senses the voltage deference between the scalp position touched by the reference electrode (blue) and the scalp position touched by another electrode (purple). Electrochemical processes at the contact surface of electrodes and skin give rise to capacitive effects. These effects happen for both stimulation and EEG electrodes. (*b*) Schematic display of an EEG measurement in vector space. The length and phase of each vector represent amplitude and phase of the corresponding time domain signal, respectively. Blue and purple vectors correspond to the voltage sensed by the reference and example EEG electrodes, respectively. Dashed vectors represent the differential EEG signal measured for an EEG electrode, which is simply the difference between voltages sensed by that electrode (purple) and the reference electrode (blue). Capacitive effects of EEG electrodes (blue and purple in (*a*)) induce small phase shifts to the voltage sensed by each EEG electrode (non-zero phase of blue and purple vectors). This effect, together with the difference in the amplitude of voltages sensed by different electrodes, leads to various phase shifts of EEG measurements. The vector model explains the negative correlation between artifact amplitude and phase deflection, which is demonstrated in topographies. The bottom topography shows the absolute value of artifact phase deflections. The top topography shows the inverse of the artifact amplitude in decadic logarithmic scale (11 Hz tASC, averaged over subjects). (*c*) Simulating heartbeat-locked phase modulations. The vector model in (*b*) generates heartbeat-locked phase modulations, when the amplitude of each electrode's voltage is modulated by each heartbeat. Topographies show the average result of simulations with reference electrodes at Fcz (left) and P8 (right). Top topographies show inverse artifact amplitude and bottom topographies depict the standard deviation of heartbeat-locked phase modulations, in decadic logarithmic scale. Channels with smaller artifact amplitude (yellow regions in top topographies) show higher heartbeat-locked phase modulations (yellow regions in bottom topographies).

although both, phase and amplitude modulations contribute to broadband tACS artifacts, the bandwidth of tACS artifacts is practically governed by the artifact's amplitude modulations.

4.2. *Underlying mechanisms*

Capacitive effects at the contact surface of EEG electrodes and skin (Fig. 5a, Bronzino and Peterson, 2015; Tyner and Knott, 1983) induce small phase shifts to the voltages sensed by different EEG electrodes (Fig. 5b, phase of turquoise and magenta vectors). Small differences in in this capacitive effect between the reference electrode and other electrodes (Fig. 5b, phase difference of turquoise and magenta vectors), together with the variable strength of tACS artifact across electrodes (Fig. 5b, length of magenta vectors), lead to variable artifact phases across different EEG channels (Fig. 5b, phase of dashed vectors). Conceptualizing this effect in vector space explains the negative correlation between artifact amplitude and phase deflection observed for EEG (Fig. 5b). Most electrodes pick up either much stronger or much weaker artifacts relative to the reference electrode. Differential recordings from these electrodes show big artifacts with phases close to zero or 180° (Fig. 5b, first and last vector drawings). On the other hand, few electrodes experience artifacts with very similar strength as the reference electrode. Recording from these electrodes show small artifacts with phases close to either 90 or -90° (Fig. 5b, middle vector drawing). This mechanism leads to the observed negative correlation between artifact amplitude and phase deflection across channels (Fig. 2b and topographies in Fig. 5b). Furthermore, because of the capacitive effect at the contact surface, electrode impedance is frequency dependent, which explains why we observed a change in phase deflection across frequencies.

The aforementioned mechanism can not only explain the observed EEG artifact phase deflections from pure linear in-phase or anti-phase versions of the stimulation current, but it may also explain the observation of heartbeat-locked and respiration-locked artifact-phase modulations. As we have shown before (Noury et al., 2016), the artifact's amplitude is modulated by physiological processes. The artifact phases of EEG measurements depends on the electrodes' capacitive effect and the artifact amplitude at each electrode (Fig. 5b). Thus, rhythmic modulations of artifact amplitude at each electrode (amplitude modulation of magenta and turquoise vectors in Fig. 5b) could lead to observed rhythmic phase modulations of the measured artifacts (phase of dashed vectors in Fig. 5b).

We tested this idea in a simulation, in which each electrode had a small random phase shift and its amplitude was modulated by each heartbeat (Fig. 5c, Materials and Methods). This simulation confirmed

that the mentioned mechanism could lead to heartbeat-locked phase modulations. As observed in the experimental measurements (Fig. 3a and b), in the simulation heartbeat-locked phase modulations were strongest for channels on the zero isoline, i.e. channels with artifact amplitudes similar to the artifact amplitude of the reference channel (Fig. 5c). This led to a negative correlation between artifact amplitude and phase-modulation strength (Spearman correlation (r) of -0.84, $p < 10^{-16}$), as also observed in the experimental measurements.

In addition to rhythmic amplitude modulation, also rhythmic impedance changes may contribute to the observed phase-modulation. In particular, rhythmic movements of EEG electrodes induced by each heartbeat may rhythmically change capacitive and resistive electrode impedances.

Capacitive effects also affect invasive electrophysiological recordings during tACS. Thus, the abovementioned model could also explain phase properties of those recordings. In fact, a recent study (Opitz et al., 2016) reported small phase shifts in invasive recordings during tACS in the range of the phase deflections reported here. Although the authors do not statistically check the relationship between signal strength and phase shifts, they report largest phase shifts at electrodes with smallest signals, and relate this to less accurate phase estimations at these electrodes. Our model suggests that the reported phase deflections result from small capacitive effects together with referencing. Moreover, according to our model, we speculate that the phase of invasive recordings should also be rhythmically modulated by heartbeat and respiration due to small rhythmic brain movements or blood volume changes. It should be noted that these phase features happen at the measurement level. In other words, we predict that neuronal tissues experience tACS currents in-phase with the stimulation current. However, neuronal responses to these electrical currents are not necessarily in-phase with the stimulation current, and might show phase shifts that depend on different parameters, including bioelectrical features of the neurons. Detailed computer simulations and invasive recordings (Ali et al., 2013; Opitz et al., 2016) are necessary to further our understanding of the phase relationship between tACS currents and induced neuronal responses.

Our results show that phase features of MEG artifacts are generally similar to phase features of EEG artifacts. However, we are not aware of any direct counterpart of the capacitive EEG effects for SQUID-based MEG that could lead to the observed phase features of MEG artifacts. These phase features may arise from the special electronics of the MEG system. One candidate could be the flux feedback loop of the SQUID circuitry. The delay of this feedback loop could potentially generate phase delays in the recordings. Another alternative is the effect of electromagnetic waves generated by oscillating stimulation currents. Usually, it is assumed that MEG signals are measured under the quasi-static condition. This is a fair assumption when measuring brain activity, because electromagnetic waves produced by time varying brain activity are negligible. However, stimulation currents are usually much bigger than electrical currents produced by brain activity. Consequently, their produced electromagnetic waves are also several orders of magnitude bigger than electromagnetic waves produced by brain activity. These electromagnetic waves are not necessarily in-phase with stimulation currents, and therefore they could induce phase shifts in artifacts measured by MEG sensors. Pinpointing the exact mechanisms underlying observed MEG phase effects remains subject to future investigations.

4.3. Consequences for artifact rejection methods

Any sub-optimality in artifact rejection leads to a decrease in the signal to noise ratio of the recovered brain signal and residual artifacts, which, in the worst case, may lead to spurious results. This is particularly important to consider because tACS artifacts are typically several orders of magnitude larger than brain signals. Optimizing artifact rejection methods requires knowledge of the nature and characteristics of artifacts. By providing these characteristics, our results pave the way for this optimization.

Widely used EEG and MEG signal-processing methods like PCA, ICA and beamforming assume a linear and time-invariant mapping between sources (artifactual or non-artifactual) and sensors. These methods have been recently used for removing stimulation artifacts (Helfrich et al., 2014; Neuling et al., 2015). However, artifact phase and amplitude features reflect a non-linear and time-varying mapping between stimulation current and tES artifacts. During normal EEG and MEG recordings without tES, discarding non-linear and time-varying properties of source-to-senor projections leads to negligible errors, because their effective strength is small relative to brain signals. However, because tACS artifacts are several orders of magnitude larger than brain signals, small non-linear and time-varying effects cause artifact components that are well on the order of, or even larger than, brain signals (Figs. 1–3; and Noury et al., 2016). These components are hard to capture with linear and time-invariant signal processing methods. In other words, using these signal processing methods for removing stimulation artifacts result in residual artifacts (Marshall et al., 2016; Noury et al., 2016). These residual artifacts are likely to lead to higher artifactual power of the processed signal at or near the stimulation frequency compared to the sham condition. Importantly, an increase in neuronal activity at the stimulation frequency is one of the targeted physiological effects of tACS. Thus, dissociating a potential physiological signal power increase from a power increase caused by residual artifacts is challenging and requires a careful assessment of the measured power changes in comparison to the effects of potential residual artifacts. Such comparisons could be done by means of computer simulations and evaluations that are based on realistic artifact models.

Another approach to artifact rejection is to design appropriate non-linear and time-varying methods. For example, in the artifact rejection method introduced by Voss et al. (2014) an optimum phase-shift is applied to the artifact estimation of each EEG channel. Although this approach is theoretically powerful, it is not able to completely remove stimulation artifacts. The main challenge in this approach is to estimate the exact amplitude and phase of the artifact over time. This is difficult because signals recorded during tES contain both artifact and brain activity. Therefore, estimations of phase and amplitude of artifact might be sub-optimal and artifact-removed signals might contain residual artifacts. Similar to the previous approach, one might be able to deal with this problem by means of computer simulations. In other words, one could estimate the strength of residual artifacts through realistic artifact models in silico, to then quantitatively assess if the observed changes in recordings during tES relative to sham recordings could be explained by residual artifacts.

We showed that artifact phase properties in EEG and MEG depend on tACS frequency. This suggests that the performance of a single artifact rejection method may vary with stimulation frequency. Therefore, artifact rejected signals of different tACS frequencies should be compared with caution. In this context, it is also important to note that, as tDCS artifacts by definition do not have any phase shift, tES artifact removal methods may perform better for tDCS as compared to tACS.

4.4. Evaluation of artifact rejection methods in silico

Whether or not all properties of stimulation artifacts are considered in the design of artifact rejection methods, their performance needs to be evaluated. One possibility for such evaluations is to apply the artifact rejection methods to the EEG or MEG data recorded during tES, and compare the results with ground truth EEG or MEG signal. Such a ground truth, especially at the stimulation frequency, is not easy to obtain, because it is not clear how tES influences the brain activity during stimulation. The alternative is to use computer simulations to simulate artifactual signals with known ground truth. For example, Helfrich et al. (2014) simulated the artifactual signals by adding a constant 10 Hz sine wave to sham recordings, and further evaluated the performance of their artifact rejection method by applying their method to this simulated data and comparing artifact-removed results with the original sham

recordings. However, from our findings, it is clear that such a simulation does not reflect the non-linear and time-varying phase and amplitude features of tES artifacts, and thus, is not suited to assess the performance of artifact rejection method. This highlights that a necessary and critical part of such simulations is an appropriate model of stimulation artifacts that captures all relevant artifact characteristics. Our results provide the basis for such simulations by characterizing phase and amplitude features of tES artifacts, and by showing how the strength of different artifact features could be estimated from EEG and MEG recordings during tES.

4.5. A model for tES artifacts

We next suggest a complex-valued model for simulating EEG and MEG recordings during tES at frequencies close to the stimulation frequency, i.e. frequencies that do not include any stimulation harmonic. This model summarizes the results presented here and in our previous paper (Noury et al., 2016):

$$Art(t) = a(t) \times e^{i\varphi(t)} \times Cur(t) \quad (1)$$

$$s(t) = Re\{Art(t)\} + b(t) \quad (2)$$

in this model, $s(t)$ is the EEG or MEG recording, $b(t)$ is the brain activity, and $Art(t)$ and $Cur(t)$ are analytic representations[1] of stimulation artifact and normalized stimulation current, respectively. $a(t)$ and $\varphi(t)$ represent each channel's time-varying artifact amplitude and phase and are defined as:

$$a(t) = a_{avr} + a_{slow}(t) + Heart(t)*h_{ah} + Resp(t)*h_{ar}(t) \quad (3)$$

$$\varphi(t) = \varphi_{avr} + \varphi_{jitter}(t) + Heart(t)*h_{\varphi h} + Resp(t)*h_{\varphi r}(t) \quad (4)$$

While a model for tACS requires both $a(t)$ and $\varphi(t)$, Eqn. (4) should be discarded for tDCS models and $\varphi(t)$ in Eqn (1) should be replaced with zero. In Eqns (3) and (4), a_{avr} and φ_{avr} represent each channel's average amplitude and average phase shift relative to the stimulation current, respectively. $a_{slow}(t)$ represents slow changes in the artifact amplitude due to slow head movements or slow changes in EEG electrode impedance. $\varphi_{jitter}(t)$ represents artifact's phase jitter, $h_{ah}(t)$ and $h_{ar}(t)$ represent mean-removed average heartbeat-locked and respiration-locked amplitude modulations, and $h_{\varphi h}(t)$ and $h_{\varphi r}(t)$ represent mean-removed average heartbeat-locked and respiration-locked phase modulations, respectively. $Heart(t)$ and $Resp(t)$ are impulse trains with impulses at moments of, respectively, ECG R-peaks and inspiration ends. In Eqns (3) and (4), * denotes temporal convolution. This operation simply applies heartbeat locked and respiration locked modulations to amplitude and phase signals with each heartbeat and respiratory effort.

To evaluate the performance of an artifact rejection method, one could first estimate the parameters of the model based on EEG or MEG signals recorded during tES. This could be done with methods presented in this and our previous papers (Noury et al., 2016). Using these parameters, a simulated version of the recorded data, $s(t)$, could be calculated. Next, the artifact rejection method should be applied to this simulated data and the results should be evaluated. It should be noted that any model parameter estimates cannot be ideal, simply because the EEG and MEG recordings that are used for estimating model parameters contain tES artifacts together with brain activity and measurement noise. That said, a versatile artifact rejection method should be able to deal with different artifact magnitudes and should not be sensitive to small changes of model parameters.

While most of the parameters in (2) and (3) could be estimated from EEG and MEG recordings, estimating $\varphi_{jitter}(t)$ is not straightforward. This is because it is not clear how much of the observed band-passed signal's phase jitter is related to the artifact and how much is related to brain activity (Supplementary Fig. 1, bottom row). Therefore, one should evaluate the performance of artifact rejection methods assuming different levels of $\varphi_{jitter}(t)$ to find the potential effect of $\varphi_{jitter}(t)$ on results of the artifact-rejection pipeline.

The abovementioned simulation could be done with different assumptions regarding the effect of tES on brain signal (i.e. $b(t)$). Four situations are possible: no effect of tES on the brain, phase-locked entrainment of brain signal, non-phase-locked increase in brain's oscillatory activity at the stimulation frequency, and a combination of the latter two cases. For the first case, $b(t)$ could be replaced with sham recordings and a simulation could be performed to check whether artifact rejected signals show any spurious effect of stimulation, i.e. a false positive result. For the other three cases, the likelihood of a false negative result could be tested by adding different levels of phase-locked or/and non-phase-locked stimulation effects to the sham recordings, applying the artifact rejection method to the simulated data (i.e. $b(t)$), and finally checking whether the induced stimulation effects are observable after the artifact removal.

It should be noted that heartbeat-locked and respiration-locked modulations of amplitude and phase might slightly vary across heartbeats and respiratory efforts. Therefore, in the case that an artifact rejection method uses heartbeat-locked and respiration-locked modulations, these variations should be estimated from recorded data and considered in simulations and evaluations. Furthermore, it should be noted that the above model only captures those aspects of tES artifacts described here and in our previous work (Noury et al., 2016). Further research should investigate if there are other artifact properties that should be incorporated into the model.

[1] The analytical representation of a signal is a complex signal with the real part equal to the signal and the imaginary part equal to signal's Hilbert transform.

Notes

N.N. and M.S. designed the research and wrote the manuscript. N.N. performed the experiments and analyzed the data.

Funding

This work was supported by the Centre for Integrative Neuroscience (Deutsche Forschungsgemeinschaft, EXC 307).

Appendix A. Supplementary data

Supplementary information related to this article can be found at http://dx.doi.org/10.1016/j.neuroimage.2017.07.010.

References

Ali, M.M., Sellers, K.K., Fröhlich, F., 2013. Transcranial alternating current stimulation modulates large-scale cortical network activity by network resonance. J. Neurosci. 33, 11262–11275. http://dx.doi.org/10.1523/JNEUROSCI.5867-12.2013.

Benjamini, Y., Hochberg, Y., 1995. Controlling the false discovery rate: a practical and powerful approach to multiple testing. J. R. Stat. Soc. Ser. B Methodol. 57, 289–300.

Berens, P., 2009. CircStat: a MATLAB toolbox for circular statistics. J. Stat. Softw.

Bronzino, J.D., Peterson, D.R., 2015. The Biomedical Engineering Handbook, fourth ed. CRC Press, Boca Raton, FL. Four Volume Set, 4 edition.

Dornhorst, A.C., Howard, P., Leathart, G.L., 1952. Respiratory variations in blood pressure. Circulation 6, 553–558. http://dx.doi.org/10.1161/01.CIR.6.4.553.

Fertonani, A., Miniussi, C., 2016. Transcranial electrical stimulation: what we know and do not know about mechanisms. Neurosci. Rev. J. Bringing Neurobiol. Neurol. Psychiatry. http://dx.doi.org/10.1177/1073858416631966.

Helfrich, R.F., Schneider, T.R., Rach, S., Trautmann-Lengsfeld, S.A., Engel, A.K., Herrmann, C.S., 2014. Entrainment of brain oscillations by transcranial alternating current stimulation. Curr. Biol. 24, 333–339. http://dx.doi.org/10.1016/j.cub.2013.12.041.

Kristiansen, N.K., Fleischer, J., Jensen, M.S., Andersen, K.S., Nygaard, H., 2005. Design and evaluation of a handheld impedance plethysmograph for measuring heart rate variability. Med. Biol. Eng. Comput. 43, 516–521.

Kuo, M.-F., Nitsche, M.A., 2012. Effects of transcranial electrical stimulation on cognition. Clin. EEG Neurosci. 43, 192–199. http://dx.doi.org/10.1177/1550059412444975.

Marshall, T.R., Esterer, S., Herring, J.D., Bergmann, T.O., Jensen, O., 2016. On the relationship between cortical excitability and visual oscillatory responses - a concurrent tDCS-MEG study. NeuroImage 140, 41–49. http://dx.doi.org/10.1016/j.neuroimage.2015.09.069.

Michard, F., 2005. Changes in arterial pressure during mechanical ventilation. Anesthesiology 103, 419–428 quiz 449–445.

Neuling, T., Ruhnau, P., Fuscà, M., Demarchi, G., Herrmann, C.S., Weisz, N., 2015. Friends, not foes: magnetoencephalography as a tool to uncover brain dynamics during transcranial alternating current stimulation. NeuroImage 118, 406–413. http://dx.doi.org/10.1016/j.neuroimage.2015.06.026.

Nitsche, M.A., Paulus, W., 2000. Excitability changes induced in the human motor cortex by weak transcranial direct current stimulation. J. Physiol. 527, 633–639. http://dx.doi.org/10.1111/j.1469-7793.2000.t01-1-00633.x.

Noury, N., Hipp, J.F., Siegel, M., 2016. Physiological processes non-linearly affect electrophysiological recordings during transcranial electric stimulation. NeuroImage 140, 99–109. http://dx.doi.org/10.1016/j.neuroimage.2016.03.065.

Nyboer, J., Kreider, M.M., Hannapel, L., 1950. Electrical impedance plethysmography a physical and physiologic approach to peripheral vascular study. Circulation 2, 811–821. http://dx.doi.org/10.1161/01.CIR.2.6.811.

Oostenveld, R., Fries, P., Maris, E., Schoffelen, J.-M., 2011. FieldTrip: open source software for advanced analysis of MEG, EEG, and invasive electrophysiological data. Comput. Intell. Neurosci. 2011, 156869. http://dx.doi.org/10.1155/2011/156869.

Opitz, A., Falchier, A., Yan, C.-G., Yeagle, E.M., Linn, G.S., Megevand, P., Thielscher, A., Deborah, A.R., Milham, M.P., Mehta, A.D., Schroeder, C.E., 2016. Spatiotemporal structure of intracranial electric fields induced by transcranial electric stimulation in humans and nonhuman primates. Sci. Rep. 6, 31236. http://dx.doi.org/10.1038/srep31236.

Pinheiro, E., Postolache, O., Girão, P., 2010. Theory and developments in an unobtrusive cardiovascular system representation: ballistocardiography. Open Biomed. Eng. J. 4, 201–216. http://dx.doi.org/10.2174/1874120701004010201.

Soekadar, S.R., Herring, J.D., McGonigle, D., 2016. Transcranial electric stimulation (tES) and NeuroImaging: the state-of-the-art, new insights and prospects in basic and clinical neuroscience. NeuroImage 140, 1–3. http://dx.doi.org/10.1016/j.neuroimage.2016.08.020.

Soekadar, S.R., Witkowski, M., Cossio, E.G., Birbaumer, N., Robinson, S.E., Cohen, L.G., 2013. In vivo assessment of human brain oscillations during application of transcranial electric currents. Nat. Commun 4. http://dx.doi.org/10.1038/ncomms3032.

Thut, G., Bergmann, T.O., Fröhlich, F., Soekadar, S.R., Brittain, J.-S., Valero-Cabré, A., Sack, A.T., Miniussi, C., Antal, A., Siebner, H.R., Ziemann, U., Herrmann, C.S., 2017. Guiding transcranial brain stimulation by EEG/MEG to interact with ongoing brain activity and associated functions: a position paper. Clin. Neurophysiol. 128, 843–857. http://dx.doi.org/10.1016/j.clinph.2017.01.003.

Tyner, F.S., Knott, J.R., 1983. Fundamentals of EEG Technology: Basic Concepts and Methods. Lippincott Williams & Wilkins.

Voss, U., Holzmann, R., Hobson, A., Paulus, W., Koppehele-Gossel, J., Klimke, A., Nitsche, M.A., 2014. Induction of self awareness in dreams through frontal low current stimulation of gamma activity. Nat. Neurosci. Adv. Online Publ. http://dx.doi.org/10.1038/nn.3719.

Witkowski, M., Garcia-Cossio, E., Chander, B.S., Braun, C., Birbaumer, N., Robinson, S.E., Soekadar, S.R., 2016. Mapping entrained brain oscillations during transcranial alternating current stimulation (tACS). NeuroImage, Transcranial Electr. Stimul. (tES) Neuroimaging 140, 89–98. http://dx.doi.org/10.1016/j.neuroimage.2015.10.024.